Transmission imaging polarimetry for a linear birefringent medium using a carrier fringe method

4 authors:

Slawomir Drobczynski
Wroclaw University of Science and Technology
41 PUBLICATIONS **167** CITATIONS

SEE PROFILE

Juan M Bueno
University of Murcia
138 PUBLICATIONS **1,316** CITATIONS

SEE PROFILE

Pablo Artal
University of Murcia
367 PUBLICATIONS **10,160** CITATIONS

SEE PROFILE

Henryk T Kasprzak
Wroclaw University of Science and Technology
137 PUBLICATIONS **968** CITATIONS

SEE PROFILE

Some of the authors of this publication are also working on these related projects:

Project   Multiphoton microscopy of ocular tissues View project

Project   ACTIVIDADES DE INVESTIGACION DEL LABORATORIO DE OPTICA DE LA UMU View project

Transmission imaging polarimetry for a linear birefringent medium using a carrier fringe method

Slawomir Drobczynski, Juan M. Bueno, Pablo Artal, and Henryk Kasprzak

We present an imaging polarimeter in transmission mode that is based on a carrier frequency method and allows a spatially resolved polarimetric description of nondichroic linear birefringent media. The apparatus incorporates a generator of polarization states in the incoming pathway and a Wollaston prism and a linear polarizer as the analyzer unit. A series of two fringe pattern images of the birefringent sample under study, corresponding to two independent polarization states of the generator unit, were recorded. From these images and by using Fourier analysis, the 2D distribution of azimuth angle and retardation were calculated. Two alternative generator units were used: (i) a linear polarizer combined with a rotatory quarter-wave plate and (ii) a liquid-crystal variable retarder. A uniform quarter-wave plate at different orientations was measured with both generator units to demonstrate the effectiveness and the accuracy of the method. The mean absolute deviations were 1.8° and 4.1° for the azimuth and the retardation, respectively, with the first generator unit, and 2.9° and 4.4° for the second one. Moreover, some nonuniform birefringent samples presenting wider ranges of azimuth and retardation were also tested.   © 2006 Optical Society of America

OCIS codes: 070.2590, 100.2650, 120.5410, 160.1190, 160.3710, 260.1440.

1. Introduction

Imaging polarimetry is used to measure spatially resolved polarization properties in optical systems and samples. It is used in a wide range of applications such as photoelasticity studies,[1–3] remote sensing,[4] turbid media and tissue analysis,[5–8] biomedical optics,[9–13] and clinical opthalmologic devices[14–16] among others. For light polarization modulation, polarimeters use rotating retardation plates,[9,13,17,18] liquid-crystal variable retarders,[8,10,11,19] Pockels cells,[14,20] or photoelastic modulators.[21,22]

The Mueller matrix provides all the polarization properties of the sample under study (i.e., birefringence, diattenuation, polarization, and depolarization).[23] For the calculation of this matrix, 16 independent combinations of polarization states are required. However, knowledge of the complete Mueller matrix is not required if one polarization property of the system is much more important than

the rest.[3,12,24] If linear birefringence is dominant, only two parameters are calculated: the retardation (the phase shift between eigenwaves after passing the sample) and the azimuth (the angle between the direction of vibration of one eigenwave and the reference axis). This noticeably reduces the number of measurements.

In this sense, polarimetry based on an interferometric technique with a carrier frequency has been reported to be useful.[25,26] The Fourier transform of the space periodic variation of the light polarization produced by a Wollaston prism is used to compute polarimetric parameters. Quan and co-workers[2] used a single image to obtain the retardation of a birefringent sample, assuming a uniform distribution of the azimuth across the sample. Oka and Kaneko[27] measured the birefringent properties of a twisted nematic liquid-crystal (LC) cell. The system incorporated four thin birefringent wedge prisms and a sheet analyzer. From a single image (containing information on one low-frequency component and three quasi-cosinusoidal components) the azimuth and the ellipticity of the polarization state of the light can be obtained.

Drobczynski and Kasprzak[28] described a theoretical carrier frequency-based method that allows the calculation of both the retardation and the azimuth of nondichroic linearly birefringent media. Here this technique has been experimentally implemented to extract polarimetric, spatially resolved information. To produce the required independent polarization
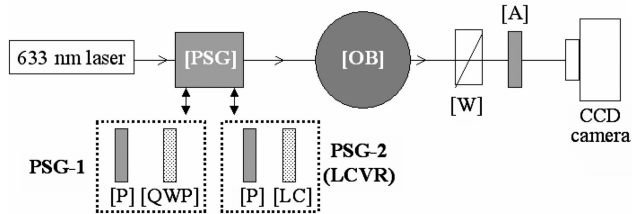
Fig. 1. Schematic diagram of the optical system. [PSG], polarization state generator; [OB], examined object; [W], Wollaston prism; [A], analyzer; [P], polarizer; [QWP], quarter-wave plate; [LC], LC cell; LCVR, liquid-crystal variable retarder.

states we used two different configurations: the classical combination of a linear polarizer and a rotatory quarter-wave plate (QWP), and a liquid-crystal variable retarder (LCVR). The results obtained with both systems are presented here. In addition, the method has been tested in samples presenting nonuniform birefringent properties.

In Section 2 we present a description of the instrument as well as the details of the theory to compute the polarization parameters associated with a birefringent structure. The results are shown in Section 3. Finally, the discussion and conclusions are presented in Section 4.

2. Methods

A. Experimental Setup and Procedure

Figure 1 presents a schematic diagram of the experimental setup. We used a 633 nm He–Ne laser as the light source. The collimated light beam first entered the generator of polarization states (PSG) able to generate the two required independent polarization states (see Subsection 2.B). After passing the sample under study (OB), the Wollaston prism (W) introduced a periodic variation in the polarization state of the light. Finally, the light beam passed through an analyzer (A) (linear polarizer at 45°) and reached the CCD camera.

Two different PSGs were used (see the insets in Fig. 1). The first was composed of a fixed horizontal linear polarizer and a rotatory QWP (PSG-1). Different polarization states were produced by orienting the fast axis of the QWP at different angles. The second PSG (PSG-2) consisted of a LCVR including a horizontal linear polarizer followed by a LC cell (with the axes 45° apart). Changes in the voltage applied to the LCVR produced different polarization states (for further information on the LCVR see Ref. 19). Both the LCVR and the image recording setup were driven by a PC.

Although the technique is essentially the same as that reported in Ref. 28, the experimental configuration was modified slightly to use the LCVR described above. A series of two fringe images of the sample under study corresponding to two independent PSG polarization states was registered. From these images and using the equations presented in the follow-

ing section, we computed spatially resolved maps of retardation and azimuth.

We first used a QWP as a test object. The fast axis was oriented at different azimuth angles within a range of 180°. Knowledge of the nominal retardation introduced by the QWP (90°) allowed us to estimate the accuracy of the instrument. Consecutive series of images were registered to test the repeatability of the proposed method. Both PSGs were used for this part of the experiment. Finally, the experimental procedure was applied to some spatially nonuniform birefringent objects such as a photoelastic medium and an *in vitro* cornea, which provided a wide range of azimuth and retardation values.

B. Theory: Calculation of the Retardation and the Azimuth

By using the Stokes–Mueller formalism,[23] both the theoretical basis of the instrument and the method to extract the parameters of polarization of a birefringent sample are explained in the following.

Each PSG unit was composed of a horizontal linear polarizer (*OX* axis) in conjunction with either a rotatory QWP or a LC cell (both elements have the same Mueller matrix).[19,23] PSG-1 and PSG-2 were able to generate the two required independent polarization states, linear horizontal and right circular, with the Stokes vectors $[\mathbf{S}_{PSG}] = [1\ 1\ 0\ 0]^T$ and $[1\ 0\ 0\ 1]^T$, respectively.

The Stokes vector of the light reaching the CCD, $[\mathbf{S}_{CCD}]$, will be a result of this product

$$[\mathbf{S}_{CCD}] = [A][W][OB]\,[\mathbf{S}_{PSG}], \tag{1}$$

where [OB], [W] and [A] are the Mueller matrices associated with the linear birefringent object, the Wollaston prism, and the analyzer.[28]

The first component of $[\mathbf{S}_{CCD}]$ is the intensity of the light recorded by the CCD. Then, for horizontal linear polarized light (produced by orienting the fast axis of the QWP at 0° or when the LC cell introduces $n\pi$ retardation, with $n \in N$) the recorded image can be expressed as

$$I_1 = T\{1 + \sin 2\alpha \cos 2\alpha(1 - \cos \delta)\cos[2\pi f_0(x + k)] \\ + \sin 2\alpha \sin \delta \sin[2\pi f_0(x + k)]\}, \tag{2}$$

where T is the transmittance of the whole system, δ is the retardation introduced by the birefringent sample, α is the azimuth angle, x is the horizontal coordinate, f_0 is the space frequency along the x axis, and $2\pi f_0 k$ is the initial phase of calculation.

Similarly, for right circular light (the fast axis of the QWP at 45° or a retardation of 90° introduced by the LC cell), the image will be given by

$$I_2 = T\{1 + \cos 2\alpha \sin \delta \cos[2\pi f_0(x + k)] \\ + \cos \delta \sin[2\pi f_0(x + k)]\}. \tag{3}$$

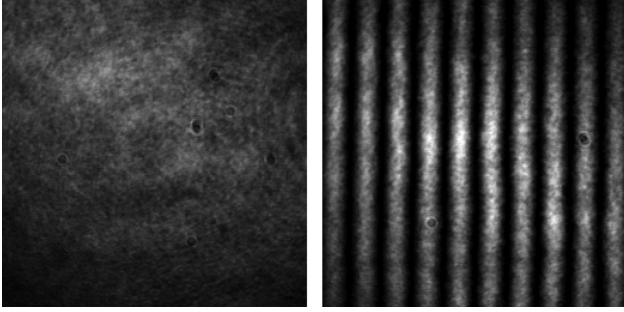Next, the Fourier transforms of the two images

Fig. 2. Images corresponding to the two independent polarization states (left, linear; right, circular) produced by PSG-1 without an object in the system. Size is 1.5 mm × 1.5 mm and gray level ranges from 0 (black) to 255 (white).
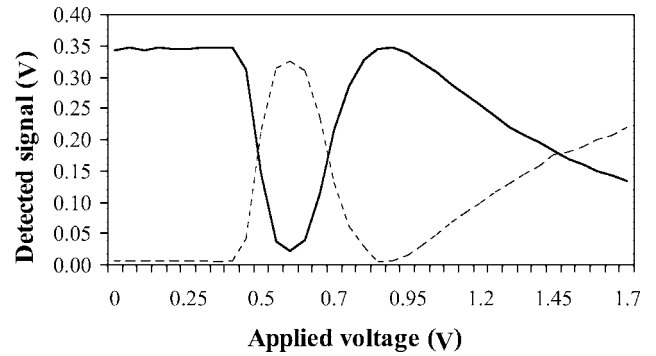

Fig. 3. Intensity signal registered during the calibration of the LCVR. Solid and dashed curves correspond to crossed and parallel linear polarizers, respectively.

were calculated. By filtering the first order in the spatial frequency spectrum, shifting it to the origin of the coordinate system by the value of carrier frequency f_0 and calculating the inverse Fourier transforms, the complex distributions of c_1 and c_2 were obtained[28]

$$\mathrm{Im}(c_1) = T\left[-\sin(2\pi f_0 k)\sin 4\alpha \sin^2(\delta/2) - \cos(2\pi f_0 k)\sin 2\alpha \sin \delta\right], \quad (4)$$

$$\mathrm{Re}(c_1) = T\left[-\sin(2\pi f_0 k)\sin 2\alpha \sin \delta + \cos(2\pi f_0 k)\sin 4\alpha \sin^2(\delta/2)\right], \quad (5)$$

$$\mathrm{Im}(c_2) = T\left[-\sin(2\pi f_0 k)\cos 2\alpha \sin \delta - \cos(2\pi f_0 k)\cos \delta\right], \quad (6)$$

$$\mathrm{Re}(c_2) = T\left[-\sin(2\pi f_0 k)\cos \delta + \cos(2\pi f_0 k)\cos 2\alpha \sin \delta\right]. \quad (7)$$

Finally, the distribution of α and δ of the object under study for $k = 0$ is

$$\alpha = \frac{1}{2}\arctan\left[\frac{-\mathrm{Im}(c_1)}{\mathrm{Re}(c_2)}\right], \quad (8)$$

$$\delta = \arctan\left[\frac{\mathrm{Re}(c_2)}{-\mathrm{Im}(c_2)\cos 2\alpha}\right]. \quad (9)$$

It appears from these equations that for $\alpha = n \times \pi/4$ $(n = 1, 2, \ldots)$ the retardation cannot be retrieved. These values are singular points for the calculation of δ. The range for the azimuth is $\pi/2$ $(-\pi/4 < \alpha < \pi/4)$ and to extend this range into the whole region of π $(-\pi/2 < \alpha < \pi/2)$ an unwrapping procedure is required to yield the continuous distribution.

However, wherever the azimuth is close to a singular point, larger errors might be present in the measured retardation. For thoses cases an alternative equation can be used:

$$\delta = \arctan\left[\frac{\mathrm{Im}(c_1)}{\mathrm{Im}(c_2)\sin 2\alpha}\right]. \quad (10)$$

3. Results

A. Calibrations

To accurately measure the polarization parameters of a sample, a calibration procedure must be performed. First, we checked if PSG-1 produced horizontal and right circular light when orienting the fast axis of the QWP at 0° and 45°, respectively. For this we used an additional linear polarizer, P2, and a photodetector. When the QWP was set at 0° and P2 at 90°, the intensity signal reaching the detector was close to zero. This ensured the entry of linear horizontal polarized light into the sample. Alternatively, when the axis of the QWP set at 45° and P2 was rotated over 90° no significant intensity changes were measured, which corroborated the generation of circularly polarized light.

As an example, Fig. 2 shows a pair of images registered in the absence of sample for the two polarization states generated by PSG-1. As expected when linear polarized light passes the Wollaston prism, no fringes are present.

For PSG-2 an independent calibration of the LCVR was performed to measure the relationship between the voltage applied to the LC and the retardation produced. The LC cell was placed between parallel and crossed linear polarizers.[19] Since the LCVR included a horizontal linear polarizer, only external polarizer P2 was used.

The intensity reaching the detector when P2 is horizontal ($\alpha_{P2} = 0°$) is given by

$$I(\delta_{LC}) = I_p\left(1 - \sin^2\frac{\delta_{LC}}{2}\right), \quad (11)$$

where I_p is the intensity entering the LC cell and δ_{LC} is the retardation introduced by the LC cell for each value of voltage. If polarizers are crossed ($\alpha_{P2} = 90°$) this intensity will be

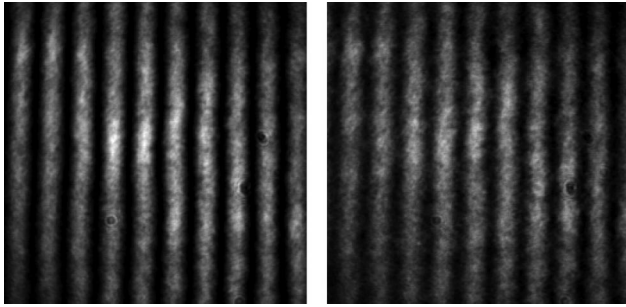$$I(\delta_{LC}) = I_p\sin^2\frac{\delta_{LC}}{2}. \quad (12)$$

Fig. 4. Polarimetric fringe images for a sample consisting of a QWP with azimuth at −30°, registered with the experimental configuration PSG-1. Left, linear polarization; right, circular polarization. Size and gray levels are the same as in Fig. 2.

Figure 3 presents the signal registered for both configurations. Points with maximum and minimum values correspond to a phase retardation equal to $n\pi$ (with $n \in N$). Points where the plots intersect are associated with a phase retardation of $(n + 1/2)\pi$ (with $n \in N$). Any pair of those values can be chosen to generate the two required polarization states. These were confirmed with the same procedure as that used for PSG-1.

B. Results for a Quarter-Wave Plate Using PSG-1 and PSG-2

As explained in Subsection 2.A, the measurements were carried out with a QWP (with a nominal retardation of 90°). Pairs of images of the QWP under study were recorded for a range of azimuth values of 180° in increments of 10°. As an example, Fig. 4 shows the two images registered when the fast axis of the QWP was oriented at −30°. From these pairs of images and by using the equations described in Subsection 2.B, the maps of azimuth and retardation were computed. The distributions of these parameters obtained from the images in Fig. 4 are depicted in Fig. 5. The average values (in degrees) for these images have been −30.3° ± 0.8° and 89.5° ± 1.5°.

The procedure was repeated for each azimuth of the QWP under test. From the maps of retardation and azimuth, the averaged value and the standard deviation across the images were calculated. In Fig. 6 the experimental azimuth values are plotted with respect to the set orientation. Individual standard
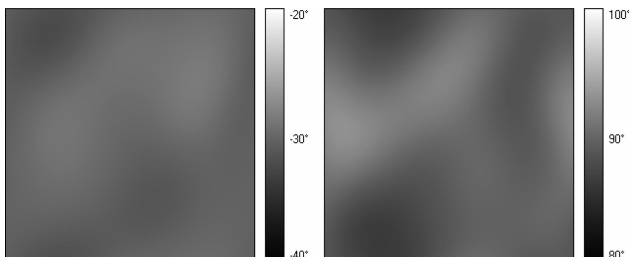
deviations varied from 0.3° to 1.4°, which indicates that the parameter is fairly constant over the sampled area. These results confirm the dynamic range of α ($-45° < \alpha < 45°$), which needs an unwrapping procedure to be expanded.

Figure 7 depicts the averaged values of azimuth and retardation for three series. Error bars are within the symbols. The solid lines correspond to the nominal values of azimuth and retardation. For both parameters the results are in good agreement with expected values. The plot shows the repeatability among measurements. Differences between the measured and the nominal averaged values ranged from 0.3° to 2.9° for azimuth and from 0.2° to 7.3° for retardation.

Similar measurements were carried out with the LCVR. The same QWP was used as a test object. For each azimuth of the fast axis of the QWP, two fringe pattern images were recorded. These corresponded to two values of the phase shift introduced by the LCVR producing the two independent polarization states. From these two images the maps for azimuth and retardation were computed.

Figure 8 shows the fringe images corresponding to a nominal azimuth of 20°. The corresponding distributions of azimuth and retardation are shown in Fig. 9. The averaged values for these maps were 22.6° ± 0.1° and 91.6° ± 0.2°, respectively.
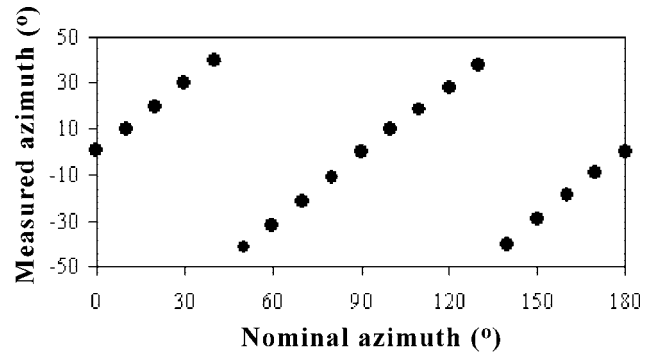
Figure 10 presents the measured azimuth and re-

Fig. 6. Measured versus nominal azimuth using PSG-1 for a QWP used as a test object. Standard deviations are within the symbols.

Fig. 5. Distribution of azimuth (left) and retardation (right) computed from images in Fig. 4. The size of each image is also 1.5 mm × 1.5 mm. The gray scales are shown on the right. Units are degrees.
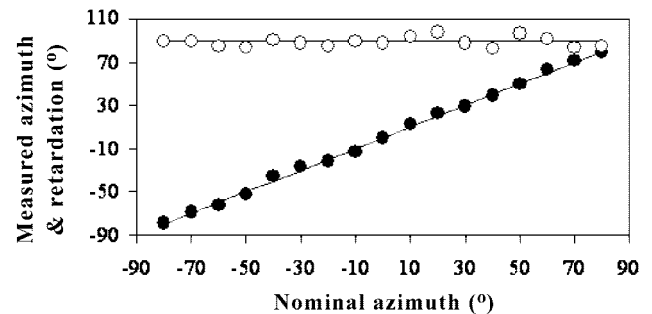

Fig. 7. Averaged values of azimuth (black symbols) and retardation (white symbols) for a QWP using PSG-1. Solid lines represent the nominal values.
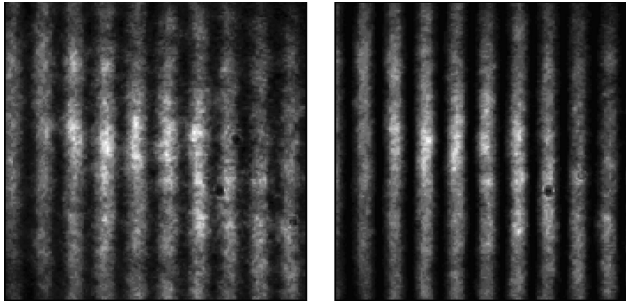
Fig. 8. Fringe images of a QWP test at 20° for linear (left) and circular (right) incoming polarizations produced by PSG-2. Gray levels and size are the same as those in Fig. 2.

Fig. 10. Measured retardation (white symbols) and azimuth (black symbols) versus nominal azimuth for a QWP using PSG-2. Each symbol is an averaged value computed from three different series. For a better comparison, lines indicate the expected values. Some data are missing due to technical problems.

tardation versus the nominal azimuth. Each symbol represents the mean value of three series. Error bars indicating the standard deviation of three repeated measurements are smaller than the symbols. The measured azimuth fits the line corresponding to the nominal data fairly well, with a largest deviation of ~5°. However, for retardation this increased up to ~10° for a nominal orientation of 30°.

C. Results for Nonuniform Samples

Once the method has been tested for a uniform and well-known birefringent sample, we will, in this subsection, demonstrate the performance of our experimental system in some nonuniform birefringent objects. For this part of the experiment we used the configuration PSG-1.

First, Fig. 11 shows the distribution for both azimuth and retardation in a LC cell. Despite the fact that this object is supposed to be fairly constant across the aperture, we decided to include these results in this subsection since this is an object different from the QWP analyzed above, which introduced retardation values much lower than the QWP.

Figure 12 presents some results on nonuniform birefringent samples, such as a photoelastic medium and an *in vitro* porcine cornea. These maps reveal how the method presented here is capable of extracting the parameters of polarization for wide ranges of azimuth and retardation.

4. Discussion and Conclusions

An imaging polarimeter in transmission mode based on an interferometric carrier frequency method has
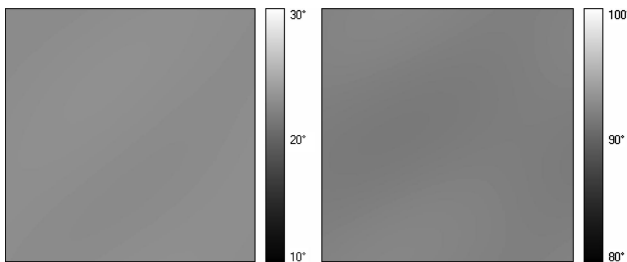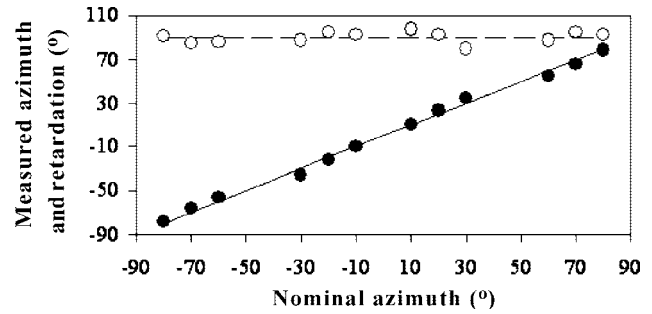
been developed to measure spatially resolved polarization parameters of nondichroic linear birefringent media. The experimental setup included a PSG unit composed of a linear polarizer combined with either a QWP or a LC cell. A Wollaston prism combined with another linear polarizer acted as the analyzer unit. When inserted in the path of the light beam, the prism produces a fringe pattern which is registered with a CCD. Two images are recorded, each corresponding to an independent polarization state produced by the PSG. A Fourier analysis of these images provides information to compute the 2D distribution of the azimuth and retardation of the sample under study.

First, this work has been centered on testing the reliability and accuracy of both the method and the experimental system in uniform samples. We have demonstrated our technique in the case of a commercial QWP oriented at different azimuths (in steps of 10° for an interval of 180°). Moreover, two different PSG units (referred to as PSG-1 and PSG-2) were tested. These generated the required polarization states. Whereas PSG-1 needed the QWP to be rotated from 0° to 45° to produce linear and circular polarizations, respectively, PSG-2 does not have any moving parts and produced the same polarization states by changing the voltage applied to the LC cell. In the second part of the experiment the method was applied to nonuniform samples.

Although the carrier frequency principle is not widely used in imaging polarimetry, the results of

Fig. 9. Maps of of azimuth (left) and retardation (right) obtained from fringe images in Fig. 8. Units are degrees. The gray scales are shown on the right for each map.
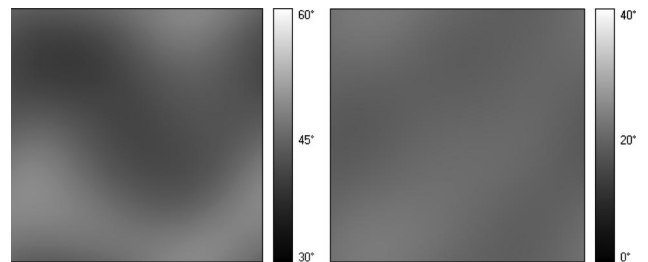

Fig. 11. Maps of azimuth (left panel) and retardation (right panel) for a LC cell. Mean values for these maps were 43.96° ± 2.6° for the azimuth, and 19.6° ± 1.2° for the retardation.
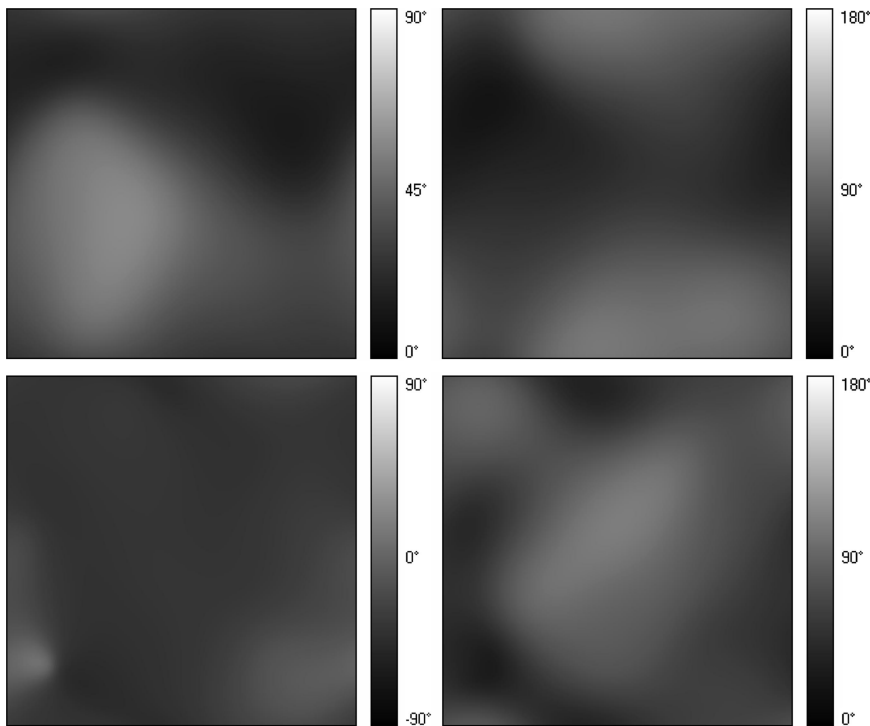
Fig. 12. Distribution of azimuth (left panels) and retardation (right panels) for a photoelastic sample (upper panels) and an *in vitro* porcine cornea (lower panels). Configuration PSG-1 was used to produce the two required polarization states.

retardation and azimuth of a birefringent sample computed from two fringe images produced by a Wollaston prism have recently been reported.[28] The authors used a fixed incident polarization state, and the modulation was produced in the analyzer by means of a LC cell. The results were based on computer simulations. Here the method has been implemented into an experimental system with some modifications because our LCVR incorporates a linear polarizer. Although in the present work the incoming beam was modulated and the analyzer kept fixed, the method is essentially the same.

Our measurements revealed fairly good agreement between the measured and the expected azimuth and a high repeatability for both PSG configurations. Despite the manual alignment of the QWP used as the test object, the mean absolute deviations were 1.8° for PSG-1 and 2.9° for PSG-2. For the retardation, these deviations were 4.1° and 4.4° for PSG-1 and PSG-2, respectively. Since the calculation of the retardation takes into account the values of the azimuth, any error in the calculation of the azimuth may affect the corresponding results for retardation. Errors in retardation might be larger when the azimuth values are close to a singular point. This source of error can be minimized by using Eq. (10). Comparing Figs. 5 and 9, it seems that PSG-2 provided more uniform images than did PSG-1. However, the accuracy in the calculation of the azimuth and the retardation was better with PSG-1.

For PSG-1, the differences between the nominal and the experimental values might be due to the typical errors of a classical rotatory polarimeter: misalignments, errors in the rotation of the QWP operating at two different angles, and the presence of

small amounts of diattenuation. For PSG-2 there are no moving parts that could introduce uncontrolled optical effects. In particular, the dependence between the measured and the real azimuths of Fig. 10 shows a systematic error in the slope, which could be attributed to a small inaccuracy in the calibration of the LCVR or some errors in the azimuth of the LCVR (let us take into account that our LCVR is a polarizer plus LC cell set). Other factors affecting the performance of a LCVR might be misalignments, or even a slight effect of the temperature on the retardation produced. The errors associated with changes in the retardation can be minimized by performing the calibration more often. Moreover, the uniformity of the PSG across the aperture could be an additonal source for error. The QWP and the LC cell used as objects were similar to those used as PSGs, which implies that for the present case the importance of this issue is not relevant.

Looking at individual orientations, the estimation of parameters was more satisfactory for PSG-1 than for PSG-2. In the case of the azimuth, the largest deviations were higher for PSG-2 (5.8°). This fact is more pronounced for the retardation, where PSG-2 presented a maximum deviation of 10.2°, whereas the corresponding value for PSG-1 was 7.3°.

Different authors have used commercially available retarders to calibrate and test the reliability of their polarimetric systems. Bueno measured a QWP in single (and double) pass with a LCVR Mueller-matrix polarimeter for different orientations of the fast axis. The retardation values ranged from 90.5° to 92.7° (from 178.2° to 179.9° for a double pass). The differences between nominal and measured azimuth were always smaller than 3°.[10,11,19] When using a LC

imaging polariscope, the parameters were extracted from the Stokes vector and errors of $\sim 3°$ in both retardation and azimuth were reported.[12]

A Berek polarization compensator was used to calibrate a polarization sensitive optical coherence tomography (OCT) system. Average errors of 7.5° and 4.8° in retardation and azimuth were reported.[29] Using a similar system Hitzenberger *et al.*[30] reported a mean absolute deviation between the set and the measured azimuth of $\sim 9.4°$ (with a maximum of 15°). The largest deviation for retardation was $\sim 4°$. Overall, the errors reported in the present work were within the ranges reported in previous literature.

On the other hand, we have presented the maps of azimuth and retardation for two nonuniform birefringent samples (a photoelastic object and an *in vitro* porcine cornea). The results show larger ranges of values for both parameters of polarization. These are the probes for the major feature of the method (spatial resolution) and confirm that our method can be used for these kinds of object.

At this point it is important to note another limitation in the method: the frequency of the fringes in images I_1 and I_2, which are important for the final spatial resolution of the computed polarization parameters. For uniform objects such as the QWP used here, the change in the spatial frequency hardly affects the results. On the other hand, for nonuniform samples the spatial frequency must be higher than the maximum gradient of the changes of azimuth or retardation. Since in the present configuration the spatial resolution is set by the angle of the Wollaston prism, some prisms might not be suitable for applications that require higher spatial resolution. In this work, the azimuth and the retardation of the sample are demodulated from the peaks in the two power spectra, which implies that the spatial variation of both parameters of polarization should change according to the period of the fringes in the images. Then, if there are some abrupt changes in areas smaller than the period of the fringes, some errors and artifacts appear in the final distribution of the polarization parameters. In particular, if the spatial frequency is lower than required, some errors in the filtering of the background function final results occur, and some details in the maps of azimuth and retardation will be missing. Moreover, the accuracy of the local estimations in the final distributions also depends on the size of the window function used when filtering the first order in the Fourier domain. However, in the nonuniform objects shown in the present work, abrupt changes in the azimuth and the retardation are not expected. In this sense the experimental configuration used for these measurements is suited for obtaining reliable spatially resolved results.

Different methods have previously been proposed for calculating the polarimetric parameters of birefringent samples. The degree of accuracy depended on the technique for measuring the optical birefringence. Probably the oldest way is to place the sample between crossed linear polarizers.[31] This method gives no information on the azimuth and requires highly birefringent samples. Another classical method is to cut the material (often crystals) into prisms in which the optical axes are aligned with the dimensions of the prisms.[32] The use of one or two photoelastic modulators as well as LC spatial light modulators was also reported to analyze birefringent samples.[12,33–35] Phase-stepping methods have also been used in photoelasticity (stress analysis) and birefringence measurements.[3,36] However, they often use more than two images to extract the retardation and the azimuth associated with birefringence.

The present method might also present some errors when samples include nonnegligible diattenuation values. In our case we have simulated the effect of nonnull diattenuation on the accuracy of our method. A QWP ($\alpha = 20°$) with three different amounts of diattenuation was simulated in a similar way to that reported in Ref. 28. Results show that the error in the determination of the azimuth and the retardation increased with diattenuation and the latter was always more affected. In particular for a diattenuation value of 0.2, the errors were 3.25% and 9.75%. Although our method has been designed for the analysis of null-diattenuation birefringent samples, the procedure can be modified to extract information on diattenuation. However, an additional image will be necessary.

LC cells are well suited for polarimetry. The details on the advantages and disadvantages of these devices can be found elsewhere.[8,10,11] They lack moving parts, are operated at low driving voltages, and significantly accelerate the recording. However, our results show that the accuracy is slightly worse than that provided by the classical rotating retarder configuration.

To conclude, the results presented establish the ability of our imaging polarimeter to measure the azimuth and the retardation of birefringent samples. This work can be seen as a first step in using the carrier frequency method in a polarimetric environment. Although the system has been used with static birefringent samples, it can also be applied to the analysis of dynamically variable samples. For the latter, the use of LCs might be of great interest. The method might be useful in the study of biological samples since many tissues present birefringence values that vary under different condiftions (thermal-induced changes, hydration, stress, and illnesses, for example). Finally, the implementation of this technique in reflection mode could help to explore optical systems with anisotropic layers or with a double-pass structure (i.e., combining the transmission and reflection modes).

References

1. J. F. S. Gomes, "Photoelasticity" in *Optical Metrology,* O. D. D. Soares, ed. (Martinus Nijhoff, 1987).

2. C. Quan, P. Bryanston-Cross, and T. Judge, "Photoelasticity stress analysis using carrier fringe and FFT techniques," Opt. Lasers Eng. **18,** 79–108 (1993).

3. J. Jaronski and H. Kasprzak, "Generalized algorithm for photoelastic measurements based on phase-stepping imaging polarimetry," Appl. Opt. **38,** 7018–7025 (1999).

4. R. Walraven, "Polarization imagery," Opt. Eng. **20,** 14–18 (1981).

5. A. H. Hielscher, A. A. Eick, J. R. Mourant, D. Shen, J. P. Freyer, and I. J. Bigio, "Diffuse backscattering Mueller matrices of highly scattering media," Opt. Express **1,** 441–453 (1997).

6. S. Jiao and L. V. Wang, "Two-dimensional depth-resolved Mueller matrix of biological tissue measured with double-beam polarization-sensitive optical coherence tomography," Opt. Lett. **27,** 101–103 (2002).

7. J. S. Baba, J.-R. Chung, A. H. DeLaughter, B. D. Cameron, and G. L. Coté, "Development and calibration of an automated Mueller matrix polarization imaging system," J. Biomed. Opt. **7,** 341–349 (2002).

8. B. Laude-Boulesteix, A. De Martino, B. Drevillon, and L. Schwartz, "Mueller polarimetric imaging system with liquid crystals," Appl. Opt. **43,** 2824–2832 (2004).

9. G. J. van Blokland, "Ellipsometry of the human retina *in vivo:* preservation of polarization," J. Opt. Soc. Am. A **2,** 72–75 (1985).

10. J. M. Bueno and P. Artal, "Double-pass imaging polarimetry in the human eye," Opt. Lett. **24,** 64–66 (1999).

11. J. M. Bueno, "Measurement of parameters of polarization in the living human eye using imaging polarimetry," Vision Res. **40,** 3791–3799 (2000).

12. J. Bueno and F. Vargas-Martín, "Measurements of the corneal birefringence with a liquid-crystal imaging polariscope," Appl. Opt. **41,** 116–124 (2002).

13. J. M. Bueno and M. C. W. Campbell, "Confocal scanning laser ophthalmoscopy improvement by use of Mueller-matrix polarimetry," Opt. Lett. **27,** 830–832 (2002).

14. B. Pelz, C. Weschenmoser, S. Goelz, J. P. Fischer, R. O. W. Burk, and J. F. Bille, "*In vivo* measurement of the retinal birefringence with regard on corneal effects using an electro-optical ellipsometer," in *Lasers in Ophthalmology IV,* R. Birngruber, A. F. Fercher, and P. Sourdille, eds., Proc. SPIE **2930,** 92–101 (1996).

15. D. S. Greenfield, R. W. Knighton, and X.-R. Huang, "Effect of corneal polarization axis on assessment of retinal nerve fiber layer thickness by scanning laser polarimetry," Am. J. Ophthalmol. **129,** 715–722 (2000).

16. Q. Zhou and R. N. Weinreb, "Individualized compensation of anterior segment birefringence during scanning laser polarimetry," Invest. Ophthalmol. Visual Sci. **43,** 2221–2228 (2002).

17. R. M. A. Azzam, "Photopolarimetric measurements of the Mueller matrix by Fourier analysis of a single detected signal," Opt. Lett. **2,** 148–150 (1978).

18. J. L. Pezzaniti and R. A. Chipman, "Mueller matrix imaging polarimetry," Opt. Eng. **34,** 1558–1568 (1995).

19. J. M. Bueno, "Polarimetry using liquid-crystal variable retarders: theory and calibration," J. Opt. A Pure Appl. Opt. **2,** 216–222 (2000).

20. F. Delplancke, "Automated high-speed Mueller matrix scatterometer," Appl. Opt. **36,** 5388–5395 (1997).

21. R. C. Thompson, J. R. Bottinger, and E. S. Fry, "Measurement of polarized light interactions via the Mueller matrix," Appl. Opt. **19,** 1323–1332 (1980).

22. G. E. Jellison, Jr., C. O. Griffiths, D. E. Holcomb, and C. M. Rouleau, "Transmission two-modulator generalized ellipsometry measurements," Appl. Opt. **41,** 6555–6566 (2002).

23. R. A. Chipman, "Polarimetry," in *Handbook of Optics,* 2nd ed. M. Bass, ed. (McGraw-Hill, 1995) Vol. 2, Chap. 22.

24. R. M. A. Azzam and N. M. Bashara, *Ellipsometry and Polarized Light* (North-Holland, 1992).

25. M. Takeda, H. Ina, and S. Kobayashi, "Fourier-transform method of fringe-pattern analysis for computer-based topography and interferometry," J. Opt. Soc. Am. **72,** 156–160 (1982).

26. Y. Otani, T. Shimada, T. Yoshizawa, and N. Umeda, "Two-dimensional birefringence measurement using the phase shifting technique," Opt. Eng. **33,** 1604–1609 (1994).

27. K. Oka and T. Kaneko, "Compact complete imaging polarimeter using birefringent wedge prisms," Opt. Express **11,** 1510–1519 (2003).

28. S. Drobczynski and H. Kasprzak, "Application of space periodic variation of light polarization in imaging polarimetry," Appl. Opt. **44,** 3160–3166 (2005).

29. J. E. Roth, J. A. Kozak, S. Yazdanfar, A. M. Rollinsm, and J. A. Izatt, "Simplified method for polarization-sensitive optical coherence tomography," Opt. Lett. **26,** 1069–1071 (2001).

30. C. K. Hitzenberger, E. Götzinger, M. Sticker, M. Pircher, and A. F. Fercher, "Measurement and imaging of birefringence and optics axis orientation by phase resolved polarization sensitive optical coherence tomography," Opt. Express **9,** 780–790 (2001).

31. M. Born and E. Wolf, *Principles of Optics,* 7th ed. (Pergamon, 1999).

32. W. L. Bond, "Measurement of the refractive indices of several crystals," J. Appl. Phys. **36,** 1674–1677 (1965).

33. F. A. Modine, R. W. Major, and E. Sonder, "High frequency polarization modulation method for measuring birefringence," Appl. Opt. **14,** 757–760 (1975).

34. C. F. Wong, "Birefringence measurement using a photoelastic modulator," Appl. Opt. **18,** 3996–3999 (1979).

35. B. L. Wang, "Linear birefringence measurement instrument using two photoelastic modulators," Opt. Eng. **41,** 981–987 (2002).

36. J. A. Quiroga and A. González-Cano, "Phase measuring algorithm for extraction of isochromatics of photoelastic fringe patterns," Appl. Opt. **36,** 8397–8402 (1997).